Scientific Research Publishing

Journal of Materials Science and Chemical Engineering, 2025, 13(9), 165-173
https://www.scirp.org/journal/msce
ISSN Online: 2327-6053
ISSN Print: 2327-6045

# A Comparative Study on Microstructure and Wear Resistance of M2 Alloy Steel Cladding Layers by High-Speed Laser Cladding and Conventional Laser Cladding

**Pengfei Sun, Dengzhi Wang***

Wuhan National Laboratory for Optoelectronics, Huazhong University of Science and Technology, Wuhan, China
Email: *D202181055@hust.edu.cn

**How to cite this paper:** Sun, P.F. and Wang, D.Z. (2025) A Comparative Study on Microstructure and Wear Resistance of M2 Alloy Steel Cladding Layers by High-Speed Laser Cladding and Conventional Laser Cladding. *Journal of Materials Science and Chemical Engineering*, **13**, 165-173.
https://doi.org/10.4236/msce.2025.139011

**Received:** August 14, 2025
**Accepted:** September 21, 2025
**Published:** September 24, 2025

## Abstract

Based on the experimental results, this study demonstrates that increasing the laser scanning speed effectively refines the microstructure of the fabricated samples, resulting in finer needle-like martensite and reduced carbide size. Although the average surface hardness decreases due to incomplete austenite-to-martensite transformation at higher speeds, the wear resistance improves significantly. The sample produced with a higher laser scanning speed exhibits the lowest wear volume, which contradicts the conventional hardness-dependent wear behavior. This enhancement is attributed to the refined microstructure, which strengthens resistance to micro-cutting and provides better load support during sliding wear. The findings suggest that microstructural refinement plays a more critical role than hardness in enhancing wear performance under the tested conditions.

## Keywords

High Speed Laser Cladding, M2 Alloy, Microstructural Evolution, Wear Performance

## 1. Introduction

High-speed laser cladding (HSLC) has recently emerged as a transformative additive manufacturing technology within the field of surface engineering [1]-[3]. Unlike conventional laser cladding (CLC), HSLC operates at substantially higher relative speeds between the cladding head and the substrate, combined with precise control of beam-powder interactions. This process facilitates rapid solidification under

extremely high throughput conditions [4]. A key characteristic of HSLC is its capacity to produce metallurgically bonded coatings that are significantly thinner, exhibit minimal dilution, demonstrate superior surface quality, and introduce markedly reduced thermal input into the substrate [5]. These attributes render HSLC particularly suitable for applications such as the repair of precision components, the deposition of high-performance thin protective layers, and the fabrication of functionally graded materials [6].

M2 high-speed steel, a representative high-carbon and high-alloy material, is extensively employed in the production of cutting tools, molds, and other critical components that demand superior wear resistance [7]-[9]. This is attributed to its martensitic matrix, which is strengthened through the addition of strong carbide-forming elements such as W, Mo, V, and Cr [10]. These elements facilitate the precipitation of hard carbides (e.g., $M_6C$ and MC types) following suitable heat treatment. However, the application of conventional laser cladding to fabricate M2 coatings faces considerable limitations. The process inherently involves high thermal input and comparatively low cooling rates, which tend to produce coarse dendritic microstructures, significant elemental segregation, and potential defects including cracks and porosity [11]. Moreover, excessive dilution can lead to deviations in the chemical composition of the clad layer, thereby adversely affecting its performance. These microstructural deficiencies ultimately restrict the improvement of mechanical properties and wear resistance in the deposited layer.

Although numerous studies have aimed at optimizing CLC process parameters for M2 coatings to alleviate these drawbacks, the inherent limitations of the technique remain challenging to fully overcome [12]. In contrast, HSLC offers a novel approach for microstructural control in M2 coatings, characterized by its extremely high cooling rates and reduced thermal input. Theoretically, HSLC is expected to promote substantial refinement of grains and carbides, diminish elemental segregation, and facilitate the formation of a more uniform and denser microstructure [13]-[15]. These advantages could lead to enhanced hardness, improved toughness, and superior wear resistance. However, systematic research on the application of HSLC to fabricate M2 high-speed steel coatings is still limited. There is a notable absence of direct and quantitative comparative studies that elucidate the microstructural and tribological differences between M2 coatings produced by HSLC and those fabricated by CLC.

Therefore, this study conducts a systematic comparative investigation to examine the differences in microstructure and wear resistance between M2 coatings fabricated by HSLC and CLC. The work aims to establish intrinsic correlations between the cladding process, the resulting microstructure, and the final performance properties. The findings are anticipated to provide a robust theoretical basis and experimental support for the application of HSLC in producing high-performance coatings.

## 2. Experimental details

### 2.1. Raw Materials

The laser cladding experiments were conducted using commercial M2 high-speed steel powders with a particle size distribution of 75 - 120 μm and #45 steel as the substrate. The chemical compositions of both the powder and the substrate are provided in **Table 1**. Prior to processing, the M2 powders were dried in a vacuum oven at 120˚C for 2 hours to reduce moisture, while the substrate surface was thoroughly cleaned with absolute ethanol to eliminate contaminants.

**Table 1.** Chemical composition (wt.%) of the powders and substrate used in this study.

| Material | Fe | Cr | W | Mo | V | C | Mn | Si |
|---|---|---|---|---|---|---|---|---|
| Powders | Bal. | 4.22 | 6.28 | 5.21 | 1.88 | 0.83 | 0.33 | 0.34 |
| Substrate | Bal. | 0.2 | - | - | - | 0.46 | 0.74 | 0.25 |

### 2.2. Fabrication Processes

Laser cladding experiments were performed using a self-developed system equipped with a continuous-wave IPG YLR-6000 fiber laser (6 kW). A schematic diagram of the experimental setup is presented in **Figure 1**. All samples were produced under consistently optimized processing parameters. For the CLC coating, the laser power was set to 2400 W, with a spot diameter of 3 mm, a scanning speed of 1 m/min, an overlap rate of 50%, and a powder feed rate of 8 g/min. The HSLC process differed primarily in the scanning speed, which was increased to 10 m/min. All samples were allowed to cool naturally at room temperature through heat dissipation.

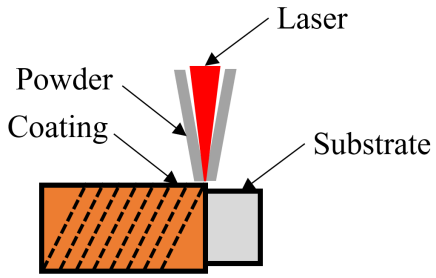


**Figure 1.** Schematic diagram of the laser cladding process.

### 2.3. Microstructural Characterization and Wear Test

Samples sectioned from the coatings were prepared for microstructural analysis through grinding, polishing, and etching with aqua regia for 5 seconds. Microstructural characterization was carried out using scanning electron microscopy (SEM). The microhardness profiles across the coating cross-sections were measured with a Vickers microhardness tester (model: Vickers-1000) under a load of 1 kg applied for a dwell time of 15 seconds.

To evaluate tribological performance, reciprocating sliding wear tests were conducted at room temperature under dry conditions. Wear test specimens with

dimensions of 10 × 10 $mm^2$ in cross-section and 6 mm in height were extracted from the coating surface. An $Al_2O_3$ ball with a diameter of 6 mm was used as the counter body. The test parameters included an applied load of 30 N, a reciprocating speed of 10 mm/s, a stroke length of 5 mm, and a total duration of 30 minutes. The wear tracks were subsequently analyzed using a three-dimensional confocal laser scanning microscope (CLSM) to quantify wear volume and examine surface morphology.

## 3. Results

### 3.1. Microstructure

**Figure 2** displays SEM micrographs of the coatings produced by different laser cladding techniques. The microstructure of all samples is composed of martensite (appearing in grey) and an interconnected network of carbides (exhibiting bright contrast). Notably, the sizes of both martensitic structures and carbides decrease with increasing laser scanning speed. In addition, the morphology of martensite transitions from coarse and bulky to a finer, needle-like form.

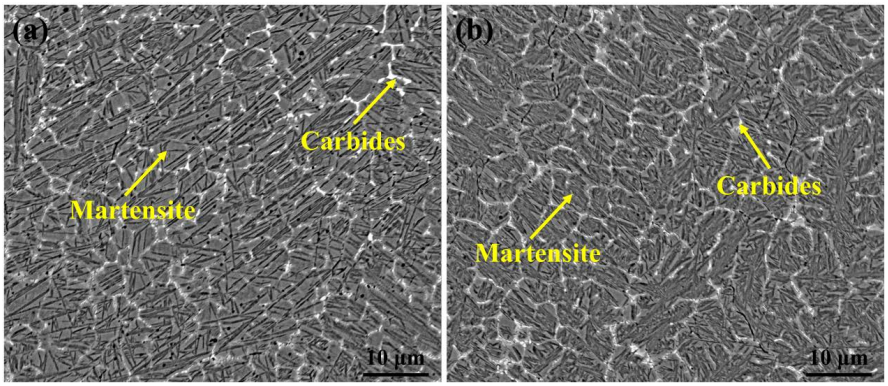


**Figure 2.** SEM images of samples: (a) CLC; (b) HSLC.

### 3.2. Hardness and Wear Performance of Samples

**Figure 3** summarizes the Vickers hardness profiles of the coatings along the depth direction. The uniformity of hardness distribution reflects the structural stability of the coating under wear conditions, while the average surface hardness correlates directly with wear resistance. As shown in **Figure 3**, all samples exhibit a relatively uniform hardness distribution along the depth, indicating good structural stability against wear. However, the average surface hardness decreases as the laser scanning speed increases from 1 m/min to 10 m/min. The measured average surface hardness values are (692.25 ± 23.82) HV for the lower speed and (657.29 ± 17.03) HV for the higher speed. This reduction is primarily attributed to the incomplete transformation from austenite to martensite, which results from the higher cooling rates associated with increased scanning speed.

**Figure 4** presents the coefficient of friction (COF) curves obtained during dry sliding wear tests. The COF evolution can be divided into two distinct stages: a

running-in stage and a steady-state stage. The contact area between the $Al_2O_3$ ball and the sample surface significantly influences the frictional behavior, with a larger contact area generally corresponding to a higher COF.

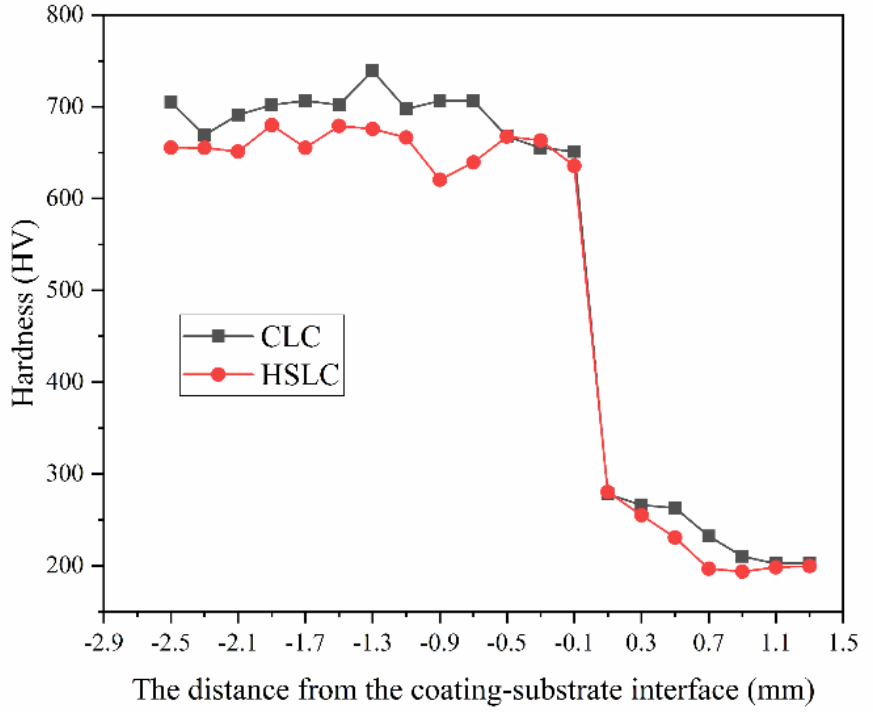


**Figure 3.** Vicker hardness along the depth (a) and average surface hardness (b) of samples.

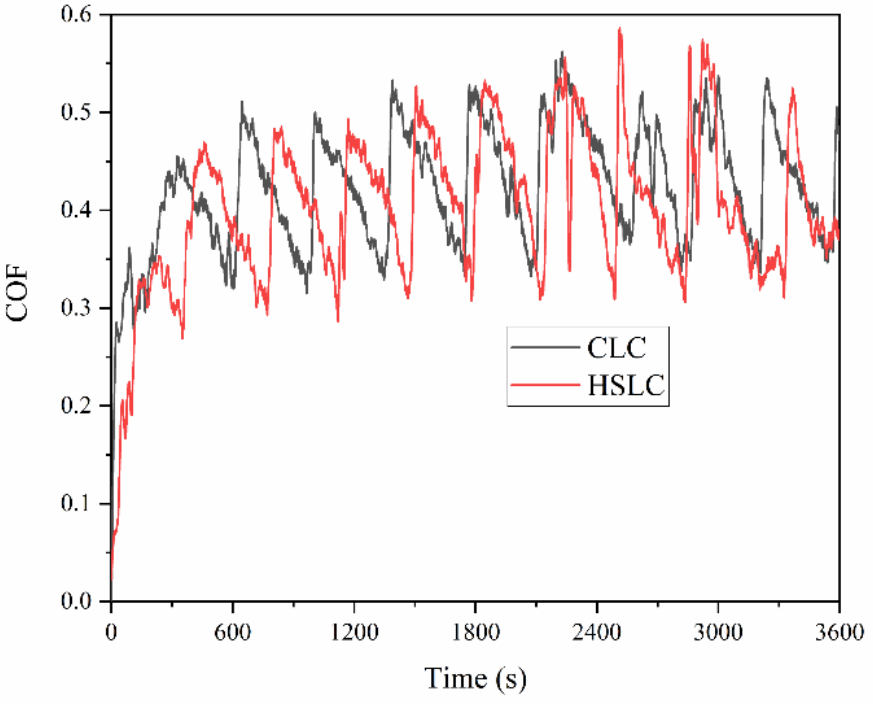


**Figure 4.** COF curves for dry friction of samples.

During the running-in stage, initial contact causes preferential wear of the softer martensitic phase compared to the harder carbides. The resulting wear-induced expansion of the contact area leads to a rapid rise in the COF. As sliding continues, plastic deformation generates wear debris. The wear process enters the steady-state stage when a dynamic equilibrium is established between debris generation and its expulsion from the contact zone. The average steady-state COF values for the samples are 0.44 ± 0.08 and 0.42 ± 0.08, respectively.

**Figure 5** and **Figure 6** present the three-dimensional morphology and two-dimensional cross-sectional profiles of the wear tracks, respectively. The 3D images reveal the presence of furrows aligned parallel to the sliding direction in all samples. As the scanning speed increases, the maximum width and depth of the wear tracks decrease. This trend, however, contrasts with the decrease in hardness observed at higher scanning speeds. The wear volume of the tracks can be calculated using the following equation [16].

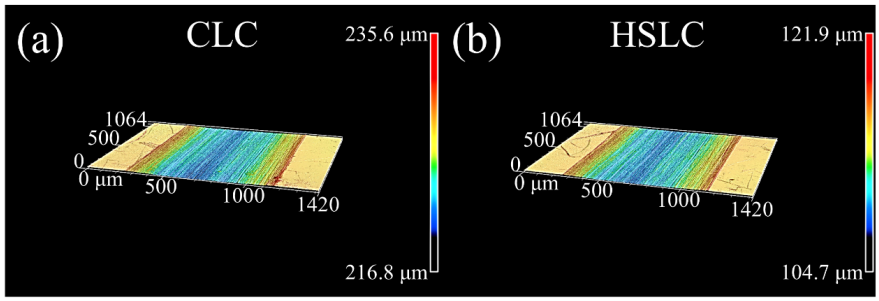


**Figure 5.** 3D morphology of the wear tracks in dry friction tests.

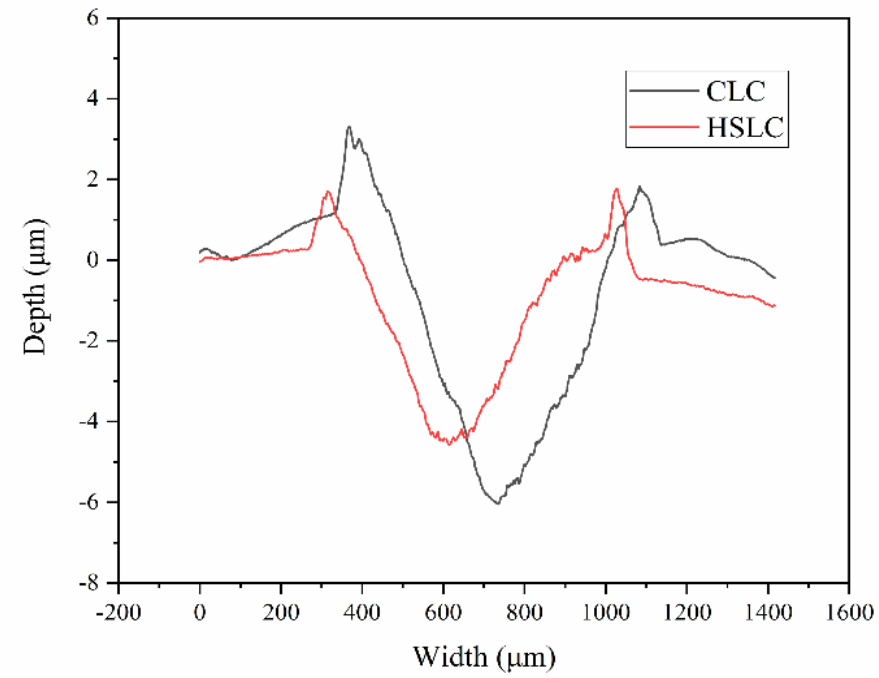


**Figure 6.** The 2D cross-section profiles (a) and feature (b) of the wear tracks in dry friction tests.

$$V = W_{q.avg} \times S$$

where $V$ represents the wear volume, $W_{q.avg}$ denotes the average cross-sectional wear area, and $S$ is the total reciprocating sliding distance. The calculated wear volumes for the samples are 0.29 $mm^3$ and 0.24 $mm^3$, respectively. Contrary to trends commonly reported in previous studies, the wear volume does not increase with decreasing hardness. The sample produced by HSLC exhibits the lowest volume loss. This behavior can be attributed to the refined martensitic matrix and carbide distribution, which enhance load-bearing capacity and mitigate the micro-cutting effect during wear.

## 4. Conclusion

The study demonstrates that increasing the laser scanning speed significantly refines the microstructure, transforming coarse bulk martensite into a finer, needle-like morphology and reducing the size of both martensite and carbides. Although this microstructural refinement results in a slight reduction in average surface hardness—attributed to the incomplete transformation of austenite to martensite—it markedly improves the wear resistance of the coating. This apparent contradiction is resolved by the refined microstructure, in which the finer martensite and well-distributed carbides enhance the load-bearing capacity and reduce micro-cutting during sliding wear, thereby leading to superior tribological performance.

## Acknowledgements

The authors would like to thank the State Key Laboratory of Material Processing and Die & Mould Technology in HUST and the Analytical and Testing Centre of HUST for microstructure characterization and wear tests.

## Data Availability

The authors do not have permission to share data.

## Conflicts of Interest

The authors declare no conflicts of interest regarding the publication of this paper.

## References

[1] Raja, D., Shetty, K. and Gopinath, M. (2025) A Study on Laser Cladding of Stellite 6 by Conventional and High-Speed Laser Cladding Process. *Surface and Coatings Technology*, **515**, Article ID: 132623.

[2] Shamsujjoha, J., Ruano, S.G., Siegfried, J., Baker, B., Thurston, M., Walluk, M., *et al.* (2025) Crack Mitigation and Wear Performance of High-Strength Steel Coatings Deposited by High-Speed Laser Cladding. *Surface and Coatings Technology*, **513**, Article ID: 132467. https://doi.org/10.1016/j.surfcoat.2025.132467

[3] Xiong, X., Taheri, M., mazaheri, h., Shaban, M., Mardani, M. and Alamri, S. (2025) Enhanced Wear Resistance of $CoCrFeNiMo_{0.3}Ta_{0.2}$ High-Entropy Alloy Coatings Fabricated by High-Speed Laser Cladding and Low-Speed Laser Cladding: The Role

of Graphene and Solidification Kinetics. *Surface and Coatings Technology*, **512**, Article ID: 132353. https://doi.org/10.1016/j.surfcoat.2025.132353

[4] Gao, Y., Li, Y., Liu, J., Wang, C., Liu, W. and Zhang, C. (2025) Research on the Elements Diffusion Behavior and Properties in Cu/W Composite Coatings by High-Speed Laser Cladding/laser Remelting. *Journal of Alloys and Compounds*, **1036**, Article ID: 181746. https://doi.org/10.1016/j.jallcom.2025.181746

[5] Wang, X., Fu, K., Ren, X., Xue, Y. and Luan, B. (2025) Investigation on the High-Temperature Molten Salt Corrosion Properties of the Inconel 625 Coatings Prepared on Q245R Steel by High-Speed Laser Cladding. *Surfaces and Interfaces*, **72**, Article ID: 107190. https://doi.org/10.1016/j.surfin.2025.107190

[6] Xu, K., Li, S., Xie, S., Cao, H., Chen, C., Cai, Y., *et al.* (2025) Microstructural Evolution, Corrosion Resistance and Antifouling Performance of $CoCrFeNiCu_x$ High-Entropy Alloy Coatings Fabricated by High-Speed Laser Cladding. *Surface and Coatings Technology*, **514**, Article ID: 132565. https://doi.org/10.1016/j.surfcoat.2025.132565

[7] Ma, H., Wang, P., Guo, Q., He, J., Luo, K., Wu, N., *et al.* (2024) Effect of $MoS_2$ Addition on the Wear Mechanism of Laser Cladding AISI M2 Coatings. *Journal of Materials Research and Technology*, **33**, 5565-5575. https://doi.org/10.1016/j.jmrt.2024.10.210

[8] Ma, H., Yang, Q., Wang, P., Wu, Z., Li, B., Du, B., *et al.* (2025) Effect of $MoS_2$ on the Microstructure Evolution of Laser Cladding M2 Coatings. *Ceramics International*, **51**, 6692-6703. https://doi.org/10.1016/j.ceramint.2024.12.113

[9] Barbosa, J.W., Martins, P.S., da Silva, E.R., Ba, E.C.T., Firpe, P.M., de Freitas Filho, R.L., *et al.* (2025) Analysis of the Tribological Behavior of Diamond-Like Carbon Coatings Applied to AISI M2 High-Speed Steel. *Thin Solid Films*, **813**, Article ID: 140622. https://doi.org/10.1016/j.tsf.2025.140622

[10] Ma, H., Wang, P., He, J., Luo, K., Du, B., Wu, N., *et al.* (2024) Differences in Hardness and Microstructure of Laser Cladding M2 Coatings. *Materials Chemistry and Physics*, **313**, Article ID: 128767. https://doi.org/10.1016/j.matchemphys.2023.128767

[11] Yuan, J., Geng, H. and Alfano, M. (2024) Multi-Response Optimization of M2 Steel Coatings Deposited by Co-Axial Laser Cladding on A2 Steel Tool Surfaces. *Journal of Materials Research and Technology*, **29**, 1102-1117. https://doi.org/10.1016/j.jmrt.2024.01.087

[12] Zhang, N., Xu, Y., Wang, M., Hou, X., Du, B., Ge, X., *et al.* (2023) M2 Coating Prepared by Ultra-High Speed Laser Cladding: Microstructure and Interfacial Residual Stress. *Materials Today Communications*, **35**, Article ID: 105638. https://doi.org/10.1016/j.mtcomm.2023.105638

[13] Liu, J., Shao, Q., Cui, X., Jin, G., Wen, X., Shi, T., *et al.* (2025) Research on *in Situ* Generation Mechanism and Tribological Properties of Superhard High Entropy Ceramic Coatings by High Speed Laser Cladding. *Ceramics International*, **51**, 27098-27103. https://doi.org/10.1016/j.ceramint.2025.03.387

[14] Yu, Y., Li, Y., Tan, N., Mou, H., Xing, Z., Liu, J., *et al.* (2025) Microstructure and Tribological Properties of Ultrasonic Vibration Assisted High-Speed Laser Cladding (CoCrNi) $88Al_6Ti_6$-cBN Coatings. *Intermetallics*, **178**, Article ID: 108644. https://doi.org/10.1016/j.intermet.2025.108644

[15] Zhou, L., Wu, H., Ma, G., Wang, H., Zhou, Y., Mou, H., *et al.* (2025) The Influence of High-Speed Laser Cladding Process Parameters on the Interfacial Structure of Nickel-Based Single-Track Cladding Layers on Copper Surface. *Optics & Laser Technology*, **183**, Article ID: 112348. https://doi.org/10.1016/j.optlastec.2024.112348

[16] Huang, Y., Chen, X., Wu, W., Wang, Y. and Wang, Y. (2025) Effect of Laser Remelting on the Microstructure and Properties of an AlCoFeNi Eutectic High-Entropy Alloy Fabricated through Double-Wire Arc Additive Manufacturing. *Journal of Alloys and Compounds*, **1010**, Article ID: 177509. https://doi.org/10.1016/j.jallcom.2024.177509